

Sunyaev-Zeldovich Cluster Counts as a Probe of Intra-Supercluster Gas

Sharon Sadeh¹

School of Physics and Astronomy, Raymond and Beverly Sackler Faculty of Exact Sciences, Tel Aviv University, Tel Aviv, 69978, Israel

and

Yoel Rephaeli

School of Physics and Astronomy, Raymond and Beverly Sackler Faculty of Exact Sciences, Tel Aviv University, Tel Aviv, 69978, Israel,

and

Center for Astrophysics and Space Sciences, University of California, San Diego, La Jolla, CA 92093-0424

Abstract

X-ray background surveys indicate the likely presence of diffuse warm gas in the Local Super Cluster (LSC), in accord with expectations from hydrodynamical simulations. We assess several other manifestations of warm LSC gas; these include anisotropy in the spatial pattern of cluster Sunyaev-Zeldovich (S-Z) counts, its impact on the CMB temperature power spectrum at the lowest multipoles, and implications on measurements of the S-Z effect in and around the Virgo cluster.

Key words: Cosmology, CMB, Clusters of Galaxies

PACS: 98.65.Cw, 98.70.Vc, 98.65.Hb

1 Introduction

As much as 30–40% of all baryons are believed to be in warm gas in large scale filamentary structures connecting clusters and superclusters (SCs) of galaxies. Observational evidence for the so-called *warm-hot intergalactic medium*

¹ E-mail: shrs@post.tau.ac.il

(WHIM) is still quite rudimentary. First systematic attempts to detect the low X-ray surface brightness enhancement that could possibly be expected from the WHIM were conducted by Persic et al. (1988, 1990) who searched the HEAO-1 A2 database in directions to a sample of SCs. In both these analyses, as well as a similar analysis of Ginga observations of the Coma-A1367 SC (Tawara et al. 1993), only upper limits were obtained on the flux from the putative intra-SC (ISC) gas. More recently, evidence for soft X-ray excess emission in regions around several clusters has been claimed by Kaastra et al. (2003), who carried out a detailed analysis of XMM-Newton line and continuum measurements of extended regions around several clusters.

X-ray emission may be expected, of course, also from the WHIM in the Local SC (LSC); analysis of the HEAO-1 A2 database led Boughn (1999) to conclude that this emission was actually detected. Adopting a simple model for the morphology of the LSC, and assuming uniform temperature and density LSC gas, Boughn deduced the mean electron density to be $n_e = 2.5 \cdot 10^{-6} (a/20 \text{ Mpc})^{-1/2} (kT_e/10 \text{ keV})^{-1/4} \text{ cm}^{-3}$, when using the specified scalings for the values of the electron temperature, kT_e , and the length of the semi-major axis of the LSC, a . More generally, Kaastra et al. (2003) have reported the detection of line and continuum WHIM emission in XMM-Newton observations of extended regions around five cluster. While the observational results on the properties of LSC gas are quite uncertain, gaseous filamentary structures seem to be a ubiquitous feature of the large scale mass distribution described by hydrodynamical simulations (e.g. Jenkins et al. 1998). Of considerable interest are the statistics and morphologies of these filaments; these are currently being quantified (e.g. Colberg et al. 2004).

The scant observational information on the WHIM and its properties in the LSC provides strong motivation for assessing the feasibility of probing it by measurements of the Sunyaev-Zeldovich (S-Z) effect (Sunyaev & Zeldovich 1972). The effect - a spectral change of the Planck spectrum due to Compton scattering of the cosmic microwave background (CMB) by electrons in clusters of galaxies - is a major cluster and cosmological probe (as reviewed by Rephaeli 1995, Birkinshaw 1999, and by Carlstrom et al. 2002). In fact, the possibility of detectable S-Z signals in directions to SCs has been considered long ago (Persic, Rephaeli & Boldt 1988, Rephaeli & Persic 1992, Rephaeli 1993), but given the substantial uncertainty in the integrated pressure of ISC, no definite predictions could be made. Measurement capabilities have greatly advanced since then, so the prospects of detecting weak S-Z signals have correspondingly improved.

Interest in the impact of ISC gas on the CMB has also increased. In particular, it has been suggested that gas in the Local Group may be responsible for the power suppression of primary CMB temperature anisotropy on large angular scales. This suppression was deduced from analyses of the COBE/DMR

(Hinshaw et al. 1996) and WMAP databases (Bennett et al. 2003). However, the estimated low Comptonization parameter of LG gas makes this suggestion quite unlikely (Rasmussen & Pedersen 2001). More recently, Abramo & Sodr e (2003) proposed that warm LSC gas may be responsible for the deduced CMB low multipole power suppression, presumably caused by coincidental alignment of a hot spot in the CMB with the line of sight connecting the Galaxy with the Virgo cluster. At the relevant spectral range of the DMR and WMAP experiments ($\sim 20 - 90$ GHz), the S-Z diminution lowers the power in the low multipoles. Clearly, for this to occur the integrated electron pressure has to be sufficiently high.

WHIM in the LSC may significantly screen our view of the CMB and S-Z sky. In addition to the possible impact on the power spectrum of CMB primary anisotropy, it will also affect the ability to measure the S-Z induced anisotropy and cluster number counts. WHIM in the LSC may appreciably increase S-Z cluster number counts. Moreover, the marked ellipsoidal shape of the LSC, and the far off-center position of the Galaxy, may result in a substantially anisotropic distribution of S-Z counts across the sky. This anisotropy in S-Z counts is obviously in addition to that generated by our motion in the CMB frame (the CMB kinematic dipole) whose effect on cluster counts was recently explored by Chluba et al. (2004).

This paper is arranged as follows: the LSC gas model, the method for calculating the directional distribution of S-Z cluster counts, and the relevant expressions for calculating the S-Z angular power spectrum, are described in section §2. The main results of the calculations are presented in §3. Additional aspects of the LSC gas model pertaining to S-Z measurements towards the Virgo cluster are discussed in §4. A general discussion follows in §5.

2 Model and Method of Calculation

The physical properties of ISC have not yet been well determined; what can be done at present is an attempt to incorporate the established observational results in a reasonable model in order to provide useful insight to guide upcoming observations, mostly of the S-Z effect. Relevant LSC properties that seem to have been *roughly* determined are the total mass, baryonic mass fraction, and its overall configuration. Knowing the baryon fraction in clusters (e.g. Carlstrom et al. 2002), and adopting the scaling to obtain the global baryonic fraction (based on hydrodynamical simulations; Evrard 1997), $\sim 10 - 14\%$, the total LSC mass, $\sim 10^{15} M_{\odot}$, then yields an estimate for the LSC WHIM mass, $\sim 3 - 5.6 \cdot 10^{13} M_{\odot}$, assuming (based on current expectations) that it comprises some 30 - 40% of the total mass. The distribution of galaxies and clusters in the LSC can be described by a spheroid of semi-axes measuring

$A = 20 \text{ Mpc}$, $B = 6.7 \text{ Mpc}$, $C = 3.3 \text{ Mpc}$ (Tully 1982); the Galaxy is on the major axis of the LSC at a distance of 15 Mpc from the center of the spheroid, where the Virgo cluster is located.

Gas in the LSC is likely to be differently distributed than the galaxies, judging by the irregular filamentary structures seen in hydrodynamical simulations. However, it is reasonable to expect that most of the WHIM is concentrated along the major axis of the LSC mass distribution. Our specific model for gas in the LSC is based on the findings of Colberg et al. (2004), who analyzed results of N-body simulations (by Kauffmann et al. 1999) in order to characterize morphologically the filaments observed in the simulations. They found that most filaments have cross sections of $1-2 \text{ Mpc}$, with the gas density decreasing outward from the major axis of the filament as $\sim r^{-2}$ beyond some scale radius r_s . The LSC gas is assumed to have an ellipsoidal configuration with semi-axes (in Mpc) of either $20 \times 1 \times 1$ or $20 \times 2 \times 2$. The highly prolate ellipsoid represents the gas ‘filamentary’ structure. The gas mean density in these structures are $n_e = 2.4 \cdot 10^{-5} \text{ cm}^{-3}$, or a factor 4 lower, respectively; its temperature is scaled to a value of 1 keV .

Clearly, the expected anisotropic morphology of ISC gas in the LSC will be reflected in anisotropic cluster counts when S-Z surveys are conducted in different sky directions. The Comptonization parameter towards the Virgo cluster, a direction which in spherical coordinates corresponds to angles $(\phi, \theta) = (0, \pi/2)$, is

$$y = \int \sigma_T \frac{kT_e}{m_e c^2} n_e d\ell = 3.4 \cdot 10^{-6} \left(\frac{kT_e}{1 \text{ keV}} \right), \quad (1)$$

whereas the corresponding value calculated for the opposite direction $(\pi, \pi/2)$ is seven times lower. The non-negligible level of the Comptonization parameter of LSC gas may modify the observed distribution of S-Z clusters across the sky; the effective y-parameter measured along a los to a cluster will have contributions from both intracluster (IC) and ISC gas, giving rise to an intensification of the apparent S-Z signal due to the cluster alone. In spherical coordinates, the path length through the ISC gas configuration as a function of position angle $\hat{n} \equiv (\phi, \theta)$ is

$$r(\phi, \theta) = \frac{\frac{30 \sin \theta \cos \phi}{A^2} + \sqrt{\left(\frac{30 \sin \theta \cos \phi}{A^2}\right)^2 - 4 \left(\frac{15^2}{A^2} - 1\right) \left[\frac{\sin^2 \theta \cos^2 \phi}{A^2} + \frac{\sin^2 \theta \sin^2 \phi}{B^2} + \frac{\cos^2 \theta}{C^2}\right]}}{2 \left[\frac{\sin^2 \theta \cos^2 \phi}{A^2} + \frac{\sin^2 \theta \cos^2 \phi}{B^2} + \frac{\cos^2 \theta}{C^2}\right]}. \quad (2)$$

The Comptonization parameter measured along this direction is then simply

$$y(\phi, \theta) = \sigma_T \frac{kT_{SC}}{m_e c^2} \cdot n_{SC} \cdot r(\phi, \theta). \quad (3)$$

where T_{SC} and n_{SC} denote the uniform temperature and electron density of the LSC gas.

The flux received from a cluster lying in the direction (ϕ, θ) is a sum of the cluster flux and the S-Z signal generated in the LSC; assuming a β -King profile for the IC gas density with $\beta = 2/3$ and an isothermal temperature distribution, the total flux at a frequency ν is

$$\begin{aligned} \Delta F(\phi, \theta) &\equiv \Delta F_C(\phi, \theta) + \Delta F_{SC}(\phi, \theta) = \\ &\frac{2(kT_\gamma)^3}{(hc)^2} \cdot \left(\frac{k\sigma_T}{m_e c^2}\right) \cdot g(x) \left[2n_0 T_0 r_c \int_0^{p\theta_c \tan^{-1} \sqrt{\frac{p^2 - (\theta/\theta_c)^2}{1 + (\theta/\theta_c)^2}}} \frac{1}{\sqrt{1 + (\theta/\theta_c)^2}} d\Omega \right. \\ &\left. + n_{SC} T_{SC} \int_0^{2\pi} \int_0^{\sigma_b} r(\phi, \theta) \theta d\theta d\phi \right], \end{aligned} \quad (4)$$

where $T_{cmb} = 2.726^\circ K$, T_0 , n_0 , T_{SC} and n_{SC} denote the temperature and density of the cluster and LSC gas, respectively, $p \equiv R_{vir}/r_c$, σ_b is the beam width, and $g(x)$ is the non-relativistic spectral form of the thermal S-Z effect, valid here owing to the relatively low temperatures of both the ISC and Virgo IC gas. At higher temperatures a relativistically correct expression (e.g. Shimon & Rephaeli 2004) must be taken into account.

The calculations were carried out in a standard Λ CDM model, specified by the parameters $\Omega_m = 0.3$, $\Omega_\Lambda = 0.7$, $h = 0.7$, $n = 1$, $\sigma_8 = 1$. We use the cluster mass function of Sheth & Tormen (2001) mass, and the temperature-mass relation

$$T = 1.3 \left(\frac{M}{10^{15} h^{-1} M_\odot} \right)^{2/3} (\Delta_c E^2)^{1/3} \left(1 - 2 \frac{\Omega_\Lambda(z)}{\Delta_c} \right) keV, \quad (5)$$

where $E^2 = \Omega_m(1+z)^3 + \Omega_\Lambda$. A non-evolving gas fraction $f_0 = 0.1$ is assumed. And since our treatment here is most relevant for the Planck all sky survey, we have selected the spectral band to be the HFI $\nu_0=353$ GHz, with $\Delta\nu = 116 GHz$; correspondingly, the beam profile is taken to be Gaussian with FWHM of $7.1'$.

Number counts are calculated based on the expression

$$N(> \Delta \bar{F}_\nu) = \int r^2 \frac{dr}{dz} dz \int_{\Delta \bar{F}_\nu(M,z)} N(M, z) dM, \quad (6)$$

where the lower limit is assigned such that the flux received from a cluster with mass M situated at redshift z exceeds the flux limit of the survey. In order to estimate the number of clusters that may be observed above a flux limit within the framework of the LSC model, the LSC S-Z flux is mapped using the second term in equation (4); the results are illustrated in the upper left-(model 1) and right-hand (model 2) panels of figure 1. The number of clusters with flux exceeding the limit ΔF_ν are then calculated using equation (6). Calculated number counts are then multiplied by $\sim 6 \cdot 10^{-4}$ to yield the number of clusters expected within square patches of sky measuring $5^\circ \times 5^\circ$. These are depicted in the lower panel of figure 1. For the detection of a cluster with a given flux to be possible, the combined S-Z flux from the cluster and the intervening LSC gas must exceed that of the measurement sensitivity. For example, if the latter is 30 mJy, then in a sky region where the S-Z flux due to the LSC is 20 mJy, the minimum detection level for a cluster is 10 mJy. Having determined the minimum flux, the expected cluster counts within a 25 square degree patch of sky in the requested direction can be read off the graph in the lower panel of figure (1).

The angular power spectrum of the S-Z effect due to LSC gas can be calculated using the usual spherical harmonic expansion of the temperature anisotropy. Here, however, the flat sky approximation is invalid due to the large angular scales involved. The basic expression is

$$a_{\ell m} = \int_0^{2\pi} \int_0^\pi \frac{\Delta T}{T}(\phi, \theta) y_{\ell m}^*(\phi, \theta) \sin \theta d\theta d\phi, \quad (7)$$

which, after projecting the three dimensional function $\Delta T/T(r, \phi, \theta)$ onto the two dimensional celestial sphere, and some algebraic manipulation, assumes the form

$$a_{\ell m} = \frac{2\sigma_T k_B T_e n_e}{m_e c^2} \int_0^{2\pi} \int_0^\pi r(\phi, \theta) \cdot y_{\ell m}^*(\phi, \theta) \sin \theta d\theta d\phi, \quad (8)$$

where $r(\phi, \theta)$ is given by equation (2). The angular power spectrum may then be easily calculated as

$$\ell(\ell + 1)/2\pi \cdot C_\ell = \ell(\ell + 1)/2\pi \cdot \frac{\sum_{m=-\ell}^{\ell} |a_{\ell m}|^2}{2\ell + 1}. \quad (9)$$

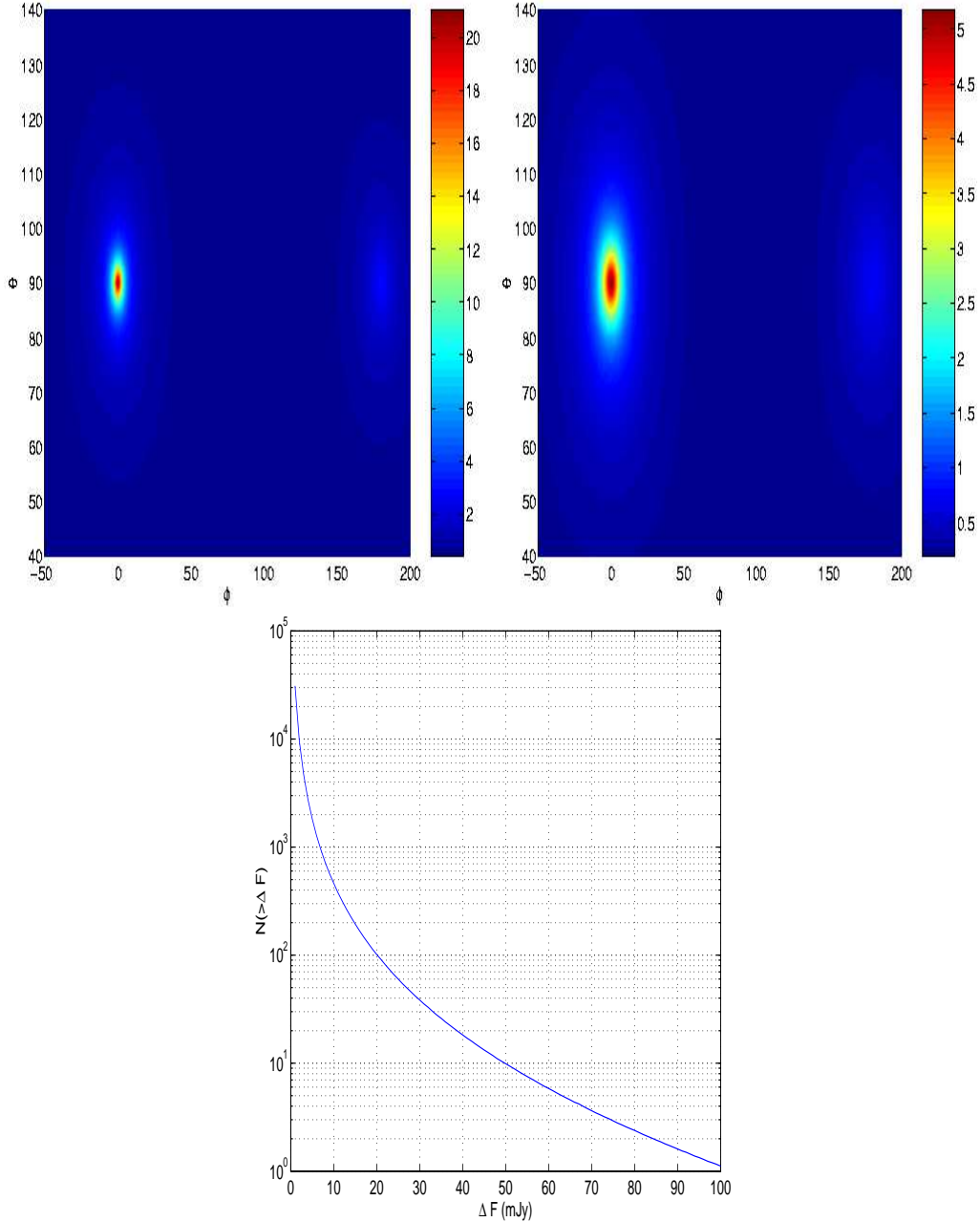


Fig. 1. Upper left- and right-hand panels: color-coded flux levels of the S-Z signal at 353 GHz (in units of mJy) from LSC gas at a density $n_e = 2.4 \cdot 10^{-5} \text{ cm}^{-3}$, and a density which is a factor 4 lower, respectively. Lower panel: number of clusters within $5^\circ \times 5^\circ$ patches of sky, above flux limit ΔF_ν .

3 Results

For flux limits of 30 mJy and 60 mJy the corresponding all-sky cluster counts sum up to $\sim 40\,000$ and $\sim 4\,300$, respectively. Assuming that the cluster population is homogeneously distributed across the sky, this amounts to ~ 24

and ~ 3 clusters in each 25 square degrees (rectangular sky region). It is important to emphasize that the number of potentially detected clusters in future S-Z surveys predicted by numerical studies is quite sensitive to the choice of parameters characterizing the background cosmology and cluster properties, and consequently, these counts merely reflect the specific modeling detailed in the last section. Now suppose that observations are conducted in the directions $\sim (\phi, \theta) = (0^\circ, 90^\circ)$ (i.e. towards the longest possible los within the LSC halo), $(5^\circ, 90^\circ)$, $(180^\circ, 90^\circ)$ (designating the direction opposite to the Virgo cluster), and, e.g., $(180^\circ, 20^\circ)$. The S-Z fluxes induced by the LSC gas in these directions are (see figure 1) $\sim 21, 7, 3, 0.5 \text{ mJy}$, respectively, implying that for a flux detection limit of 30 mJy clusters will be detected if their S-Z signals exceed the complementary values $(9, 23, 27, 29.5 \text{ mJy}$, respectively) in these directions. The corresponding limiting values for a mean gas density of $n_e = 6 \cdot 10^{-6} \text{ cm}^{-3}$ are $\sim 25, 27, 29.3, 29.7 \text{ mJy}$, respectively.

The number of clusters that could be detected in these directions, i.e., those which meet the detectability criterion, can be easily read off the diagram in figure 1. For example, an experiment with a detection limit of 30 mJy yields $\sim 570, 73, 50, 40$ clusters per 25 square degrees. The corresponding counts for the larger ellipsoid (with gas density lower by a factor of 4) are $\sim 60, 50, 40, 40$. A limiting flux of 60 mJy yields counts of $\sim 20, 8, 7, 6$ in the first case, and $\sim 6 - 8$ for all directions in the second case. While these estimates of the cluster number counts are substantially uncertain, and the fact that there is also considerable variation along different los across 25 square degrees (particularly towards both ends of the spheroid major axis), the results nonetheless demonstrate the possible impact of LSC gas, especially in a survey with 30 mJy flux limit, and in direction to the Virgo cluster. The difference between counts along los in the Virgo region and those in other directions markedly exceed the statistical uncertainty (of a purely Poissonian distribution of clusters).

The angular power spectrum of the S-Z effect induced by LSC gas is illustrated in figure 2. The maximum power level is significantly lower than the corresponding values found by Abramo & Sodr . This is due to our lower values of the density and temperature, each lower by a factor of ~ 2 than their values ($5 \cdot 10^{-5} \text{ cm}^{-3}$, and 2 keV), and the very different LSC gas configuration assumed by Abramo & Sodr , which is reflected in a different distribution of power among the explored multipole range. In particular, more power is seen at higher multipoles (with regard to Abramo & Sodr 's results), which is expected owing to its highly prolate morphology. Consequently, given the substantial uncertainty in the properties of ISC gas, one cannot convincingly argue that the observed suppression of the primary CMB temperature power spectrum is due to Compton scattering in the LSC.

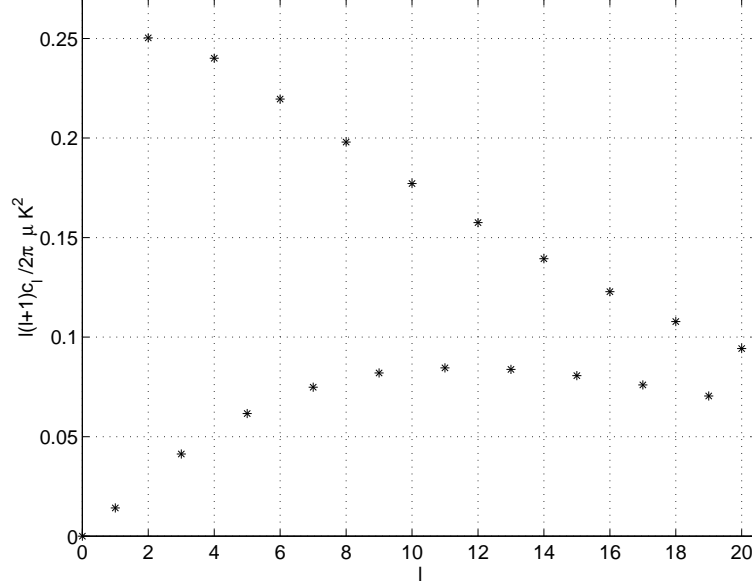


Fig. 2. The angular power spectrum of the S-Z effect induced by the gaseous LSC halo.

4 Implications for the Virgo Cluster

The central location of Virgo in the LSC implies that measurement of the S-Z effect in this cluster will likely include a substantial contribution from LSC gas. The Comptonization parameter measured along the direction (ϕ, θ) is

$$y = \sigma_T \frac{kT_{SC}}{m_e c^2} n_{SC} r(\phi, \theta) + 2\sigma_T \frac{kT_0}{m_e c^2} n_0 r_c \ell(\phi, \theta), \quad (10)$$

where $r(\phi, \theta)$ is given in equation (2) and

$$\ell(\phi, \theta) = \left[1 + \left(\frac{\theta}{\theta_c} \right)^2 \right]^{-\delta} \cdot \sqrt{p^2 - (\theta/\theta_c)^2} \cdot H_2F_1 \left[\frac{1}{2}, \delta, \frac{3}{2}, \frac{-(p^2 - (\theta/\theta_c)^2)}{1 + (\theta/\theta_c)^2} \right], \quad (11)$$

is the integrated line of sight through the Virgo cluster. Here θ_c is the core radius, $\delta \equiv 3/2\beta\gamma$ where γ is a polytropic index, p is the virial to core radius ratio, and H_2F_1 is the hypergeometric function. The main gas configuration in Virgo is centered on the giant elliptical M87, to which we refer here. Excluding a relatively small region in the center of M87, the gas is taken to be isothermal with a (King) β density profile, having (Matsumoto et al. 2000) $n_0 = 0.019 \text{ cm}^{-3}$, $T_0 = 2.28 \text{ keV}$, $r_c = 0.014 \text{ Mpc}$, $p = 125$, and $\beta = 0.4$. The magnitude of y along the central Virgo los increases by $\sim 20\%$ due LSC gas, its gradient across the cluster is appreciably shallower than would be expected from the intrinsic density profile, and the cluster seems slightly larger due to

the enhancement of the cluster Comptonization parameter.

The combined motion of the earth towards Virgo and the motion of the LSC in the CMB frame accounts for the dipole term; the deduced velocity is $\sim 600 \text{ km s}^{-1}$ in the direction ($\ell = 264^\circ, b = 48^\circ$) in galactic coordinates (Fixen et al. 1996). The temperature change generated by the dipole in the direction of Virgo is $\Delta T/T \sim 1.8 \cdot 10^{-3}$, whereas the combined S-Z temperature change due to the LSC halo and Virgo cluster peaks at $\Delta T/T \sim 5 \cdot 10^{-5}$. Clearly, the dipole may interfere with S-Z measurements of the Virgo cluster and should therefore be taken into account. This would generally be the case for large angular diameter clusters, across which the dipole gradient can be significant. The temperature change due to the dipole term is simply

$$\left(\frac{\Delta T}{T}\right)_{dipole} \equiv \frac{T_{obs} - T_0}{T_0} = \frac{v}{c} \cos \theta, \quad (12)$$

whereas the temperature change due to the thermal S-Z effect in the R-J region is $\Delta T/T = s(x) \cdot y$, where $s(x) = x/\tanh(x/2) - 4$. In order to be able to compare the contributions of both effects to the temperature change, the galactic coordinates specified above are converted into equatorial coordinates, and transformed such that the Virgo cluster lies in the direction ($\phi = 0^\circ, \theta = 90^\circ$). In this coordinate system the velocity vector points at $\sim (\phi = 340^\circ, \theta = 110^\circ)$. Figure 3 illustrates the relative temperature change ($\Delta T/T$) due to the LSC+Virgo S-Z signal, and the latter combined with the CMB dipole $(\Delta T/T)_{dipole} + (\Delta T/T)_{SC+Virgo}$ within a $10^\circ \times 10^\circ$ patch of sky centered around the Virgo cluster. The relative temperature change due to the dipole does not change considerably across the patch due to its small angular size and the fact that the angle formed between the dipole and the vector pointing at Virgo lies within the range $21^\circ \leq \gamma \leq 35^\circ$, at a significant angular distance from the direction at which the cosine term of the dipole has the steepest slope, $\gamma = 90^\circ$. The angle between the two vectors can be calculated using

$$\cos \gamma = \cos \theta_1 \cos \theta_2 + \sin \theta_1 \sin \theta_2 \cos (\phi_1 - \phi_2). \quad (13)$$

The combined relative temperature change is still dominated by the dipole term, although its profile is now deformed due to the S-Z induced temperature change. In particular a 'warm spot' may be seen in the direction of Virgo (which translates into an enhancement of $\sim 3\%$ of the temperature change due to the dipole term in this direction), by virtue of the fact that at a frequency of 353 GHz the cluster behaves as a source for CMB photons. Consequently, it is obvious that the dipole term must be taken into account in measurements of S-Z signals in nearby clusters.

The impact of LSC gas on measurements of the S-Z towards the central Virgo region is appreciable only when observations are made in a survey mode - such

as planned with PLANCK - with relatively short scan time over the region, and consequently insufficient sensitivity to remove such an LSC component. Clearly, the additional signal due to LSC gas can largely be subtracted out when pointed observations are made with a suitably selected beam-through pattern.

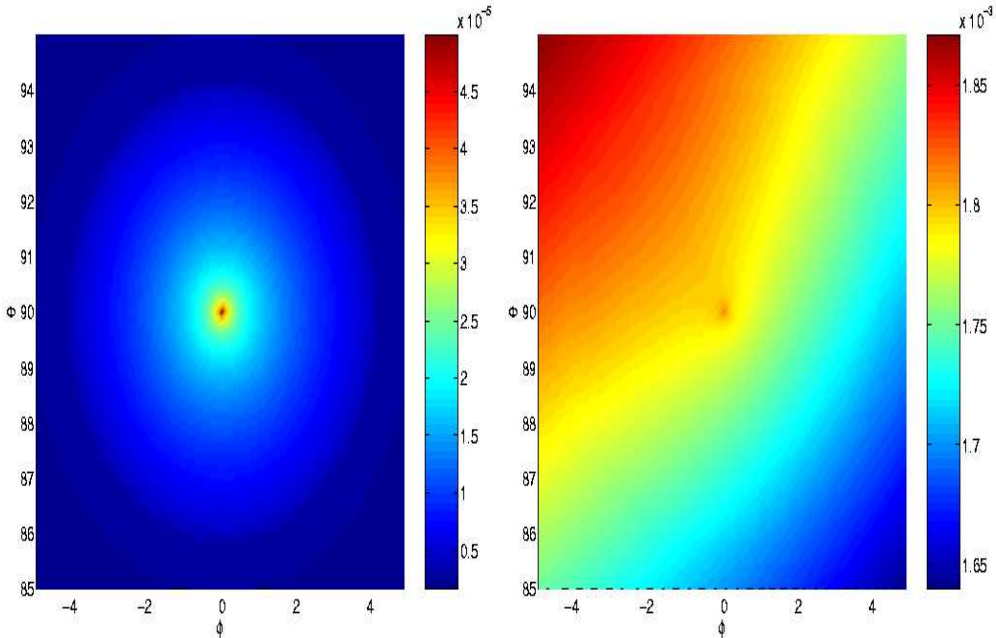


Fig. 3. The distribution of the relative temperature change around the Virgo cluster due to IC and ISC gas (left-hand panel), and combined with the temperature change induced by the CMB dipole term (right-hand panel).

5 Discussion

Although there is yet no unequivocal observational evidence for the WHIM, theory and hydrodynamic cosmological simulations indicate that it is highly prevalent and constitutes a substantial fraction of the baryonic mass fraction. Currently available observations of WHIM in several cluster regions imply appreciable levels of the Comptonization parameter, $\sim 10^{-5}$, comparable to values in most clusters. Even though we used a simplified model for the WHIM in the LSC in order to explore some of its consequences, we consider the results presented here to be qualitatively valid. In fact, our approximation of the WHIM filamentary structure by an ellipsoidal configuration (with a large volume) quite likely underestimates its S-Z impact, given the basic premise that it constitutes an appreciable fraction of the baryon mass of the LSC. As indicated by morphological analyses of such filaments seen in hydrodynamical simulations, their density grows towards the central axis, such that a clear preferential direction marked by the axis can generate even higher S-Z signals

along this direction. Moreover, the adopted symmetric morphology underestimates the density along the main axis in direction to Virgo as there is no cluster in the opposite side of the LG-Virgo direction.

Several potential observational consequences of the presence of such gaseous component have been discussed in this paper: the angular power spectrum of the induced S-Z signal has been calculated and shown to be rather low, particularly with regard to what has been speculated in the literature as a possible explanation for the suppression of primary CMB power on the lowest multipoles. While we cannot rule out a suppression at the claimed level, we do not find this to be very likely. The effect of LSC gas on directional S-Z cluster counts is proportional to the l crossing the volume of gas in the LSC. On the other hand, a definite prediction can be made that the distribution of S-Z cluster counts across the sky will be determined to be anisotropic close to the level estimated here. The impact is relatively significant owing to the highly non-linear form of the mass function; a relatively low S-Z flux induced by intervening LSC gas may give rise to a considerable increase in the number of potentially detected clusters. This is in particular true in light of the decidedly higher abundance of low-flux S-Z clusters predicted by the mass function. Needless to say, this effect is most noticeable along the main axis towards Virgo. S-Z measurements of the Virgo cluster may also be affected by the presence of the WHIM, as well as by the dipole distribution of the primary CMB temperature anisotropy. This is even more relevant to measurements of the kinematic effect, since the induced temperature change does not depend on the temperature of the LSC gas, which tends to be lower than typical IC temperatures. These effects will have to be taken into account in realistic analyses of the S-Z signal from the Virgo cluster.

Finally, although observational evidence for the WHIM is still scarce, it is interesting to use the currently available data to assess its potential of generating a significant S-Z signal towards other SCs. Kaastra et al. (2003) list five clusters (A1795, Sersic 159-03, MKW3s, A2050, A2199) reported to include a WHIM component, modeled to lie within a spherical halo, be isothermal and of homogeneous density. For each cluster they list the WHIM electron density, temperature, and size, such that the Comptonization parameter along the radius of the spherical halo can be easily calculated. They all turn out to lie within the range $y \sim (0.4 - 0.8) \cdot 10^{-5}$, i.e. near the level taken here for the LSC. Thus, the S-Z consequences of ISC gas we considered here are likely to be relevant in other nearby SCs, but obviously on smaller angular scales.

References

- Abramo L.R. & Sodr e L.Jr., 2003, (astro-ph/0312124)
- Bennett C.L., Halpern M., Hinshaw G., Jarosik N., Kogut A., Limon M., Meyer S.S., Page L., Spergel D.N., Tucker G.S., Wollack E., Wright E.L., Barnes C., Greason M.R., Hill R.S., Komatsu E., Nolte M.R., Odegard N., Peiris H.V., Verde L., & Weiland J.L., 2003, Ap. J. Supp. , 148,1 (2003ApJS..148....1B)
- Birkinshaw M., 1999, Phys. Rep. , 310, 97 (1999PhR...310...97B)
- Boughn S.P., 1999, Ap. J. , 526, 14 (1999ApJ...526...14B)
- Carlstrom J.E., Holder J.P., & Reese E.D., 2002, Annu. Rev. Astron. Astrophys. , 40, 643 (2002ARA&A..40..643C)
- Chluba J., H utsi G., & Sunyaev R.A., 2004, astro-ph/0409058
- Colberg J.M., Krughoff K.S., & Connolly A.J., 2004, astro-ph/0406665
- Evrard A.E., 1997, MNRAS , 292, 289 (1997MNRAS.292..289E)
- Fixen D.J., Cheng E.S., Gales J.M., Mather J.C., Shafer R.A. & Wright E.L., 1996, Ap. J. , 473, 576 (1996ApJ...473..576F)
- Hinshaw G., Banday A.J., Bennett C.L., Gorski K.M., Kogut A., Smoot G.F., 1996, Ap. J. , 464, L17 (1996ApJ...464L..17H)
- Jenkins A. et al. , 1998, Ap. J. , 499, 20 (1998ApJ...499...20J)
- Kaastra J.S., Lieu R., Tamura T., Paerels F.B.S, & den Herder J.W.A., 2003, Astron. Astrophys. , 397, 445 (2003A&A...397..445K)
- Kauffmann G., Colberg J.M., Diaferio A., & White S.D.M., 1999, MNRAS , 303, 188 (1999MNRAS.303..188K)
- Matsumoto H., Tsuru T.G., Fukazawa Y., Hattori M., & Davis D.S., 2000, Publ. Astron. Soc. Japan , 52, 153 (2000PASJ...52..153M)
- Persic M., Rephaeli Y., & Boldt E., 1988, Ap. J. , 327, L1-L3 (1988ApJ...327L...1P)
- Persic M., Jahoda K, Rephaeli Y., Boldt E., Marshall F.E, Mushotzky R.F., & Rawley G., 1990, Ap. J. , 364, 1 (1990ApJ...364....1P)
- Rasmussen J. & Pedersen K., 2001, Ap. J. , 559, 892 (2001ApJ...559..892R)
- Rephaeli Y., 1993, Ap. J. , 418, 1 (1993ApJ...418....1R)
- Rephaeli Y., 1995, Annu. Rev. Astron. Astrophys. , 33, 541 (1995ARA&A..33..541R)
- Rephaeli Y. & Persic M., 1992, MNRAS , 259, 613 (1992MNRAS.259..613R)

- Sheth R.K. & Tormen G., 2001, MNRAS , 323, 1 (2001MNRAS.323....1S)
- Shimon M. & Rephaeli Y., 2004, NewA , 9, 69 (2004NewA....9...69S)
- Sunyaev R. & Zeldovich Y., 1972, Comments. Astrophys. Space Phys. , 4, 173
(1972CoASP...4..173S)
- Tawara Y., Kawada M., & Koyama K., 1993, Publ. Astron. Soc. Japan , 45, 661
(1993PASJ...45..661T)
- Tully R., 1982, Ap. J. , 257, 389 (1982ApJ...257..389T)